INTERNATIONAL JOURNAL FOR NUMERICAL METHODS IN FLUIDS
Int. J. Numer. Meth. Fluids 2006; **51**:881–895
Published online 28 December 2005 in Wiley InterScience (www.interscience.wiley.com). DOI: 10.1002/fld.1142

Numerical simulations of interfacial instabilities on a rotating miscible droplet in a time-dependent gap Hele–Shaw cell with significant Coriolis effects

Chen-Hua Chen[1,2,‡] and Ching-Yao Chen[1,*,†]

[1]*Department of Mechanical Engineering, National Yunlin University of Science and Technology, Yunlin, Taiwan, ROC*
[2]*Department of Automation Engineering, Nan Kai Institute of Technology, Nantou, Taiwan, ROC*

SUMMARY

Interfacial instability of a rotating miscible droplet with significant Coriolis force in a Hele–Shaw cell is simulated numerically. The influences of the relevant control parameters are first discussed qualitatively by fingering patterns. More vigorous fingerings are found at higher rotational effects, a lower viscosity contrast and a weaker effective surface tension (Korteweg constant). For a time-dependent gap Hele–Shaw cell, a higher cell lifting rate makes the rotating droplet bear an inward straining flow, which leads to fingering enhancement. On the contrary, a higher pressing rate provides more stable effects by additional squeezing outward flow. A quantitative analysis between the Coriolis effects and tilting angles of fingers is addressed. For arbitrary combinations of all relevant control parameters, the values of tilting angles follow a nearly linear relationship with the Coriolis effects. We estimate the correlation between the relevant control parameters (dimensionless Coriolis factor Re, viscosity parameter R, cell lifting rate a) and tilting angles (θ) of fingers that can be approximated as $\theta = (0.0047\sqrt{Pe}/R + 18.2a)Re$ for significant Korteweg stresses. Copyright © 2005 John Wiley & Sons, Ltd.

KEY WORDS: miscible fluids; rotating Hele–Shaw cell; fingering instabilities; Coriolis force

1. INTRODUCTION

The dynamics of interfacial stability in a Hele–Shaw cell, or porous medium, are investigated intensively since the pioneer works by Hill [1] and Saffman and Taylor [2]. The viscous fingering instability arises when a less viscous fluid displaces a more viscous one in the narrow gap between two flat parallel plates, known as a Hele–Shaw cell. If the flow oc-

*Correspondence to: Ching-Yao Chen, Department of Mechanical Engineering, National Yunlin University of Science and Technology, 123 University Rd., Section 3, Touliu, Yunlin 640, Taiwan, ROC.
†E-mail: chingyao@yuntech.edu.tw
‡E-mail: chenhaw@nkc.edu.tw

Contract/grant sponsor: ROC NSC; contract/grant number: 93-2212-E-224-006

Received 2 September 2005
Revised 21 October 2005
Accepted 30 October 2005

curs in rectilinear channels, the less viscous fluid makes the shape of a long, smooth bubble [1, 2]. On the other hand, branched and much more intricate interfacial patterns are formed if the less viscous fluid is injected through a hole located on the upper plate, and flows radially [3]. Many theoretical and experimental studies have been performed and have led to a good understanding of the basic physical mechanisms in both geometries. Another Hele–Shaw problem is the rotating cell, which is rotated around an axis perpendicular to the plane of the flow. In this situation, the interfacial instability is driven by centrifugal forces acting on the interface separating fluids of different densities. Stronger unstable mechanism is expected if the heavier fluid, usually more viscous, is the driving fluid and moves away from the centre. The competition of these two counter-effective mechanisms, viscously stable and density unstable, leads to the determination of interfacial instabilities.

In recent years, the rotating Hele–Shaw flows have been the subject of intensive studies [4–14] due to their potential applications to the technology of spin-coating, i.e. precious metals for electronic wafers, or organic solvents for cleaning purposes. In the common practices of the spin-coating process, a liquid drop is initially deposited on the top of a rotating target substrate, and is spread outward by centrifugal force [15, 16]. Since the coating layer is extremely thin, the approximation by lubrication theory yields a similar physical phenomenon to Hele–Shaw equations. Thus, the process of spin-coating bears a great resemblance to a rotating droplet in a Hele–Shaw cell. However, based on this theory, most of the problems being studied focus on the evolution of the interface in constant-gap spacing cells. The time-dependent gap Hele–Shaw flow, where the upper plate is lifted or pressed uniformly and the plates remain parallel to each other during the process, has been one of the subjects for recent studies [17–19]. In such types of problems, a simple radial geometry flow in lifting cell has been investigated theoretically [17, 19] and experimentally [18]. They have reported that the lifting puts the fluid under a lateral straining flow that induces an unstable inward driving force and forms visually striking fingering patterns. However, these studies are results from a stationary droplet. For further investigation, in this work, we will focus on a rotating miscible droplet in a time-dependent gap Hele–Shaw cell.

In the modern micro-fabrication practice, the spin-coating takes place at high rotational Bond number [15]. Wang and Chou [15] experimentally study the fingering instability of spinning-droplet at high rotational Bond number and report that the maximum attainable radius may strongly depend on Reynolds number. Thus, the Coriolis force plays an important role for spinning flow, which arouses much interest in investigating the effects of Coriolis force. Recent research studies simulations of immiscible [5] and miscible [9] flows in a rotating Hele–Shaw flow, accounting for the Coriolis forces. Chen and Liu [9] report that the miscible interface is found to be more stable at higher Coriolis factors without an addition injection. However, with an additional injection, the interfacial fingerings are suppressed but the significant body distortion is observed. In these studies, the effects of significant Coriolis forces have yet been investigated thoroughly. Thus, in this numerical study we focus on a rotating miscible droplet in a time-dependent gap Hele–Shaw cell with significant Coriolis effects. In addition, we also study the effects of unconventional miscible effective interfacial tension, or the so-called Korteweg stresses [19–23]. The similarities between the miscible Korteweg stresses and conventional surface tension amid an immiscible interface had been verified qualitatively [19–22] and quantitatively [23]. To conclude the study, a quantitative correlation between relevant control parameters and tilting angles of fingers caused by the effects of significant Coriolis forces will be established. The outline of this paper is as

follows. After the formulation of the physical problem and review of the computational technique in Section 2, Section 3 focuses on the computational results and their interpretations. Conclusions are provided in Section 4.

2. PHYSICAL PROBLEM AND GOVERNING EQUATIONS

We investigate the interfacial instability of a heavier (density ρ_{h}) and more viscous (viscosity μ_{h}) droplet with an initial diameter D_o, which is surrounded by a miscible fluid with less density and viscosity, denoted as ρ_{l} and μ_{l}, respectively, in a rotating Hele–Shaw cell with a time-dependent gap. The cell rotates uniformly around its symmetry axis. In this confined environment, the flow takes place in narrow space between two flat plates, where the upper plate is lifted up or pressed down at a specified rate, and the lower plate is held fixed. The initial plate spacing is represented by b_o, and the plate–plate distance is denoted by $b(t)$ with the change of time t. As in Reference [17], we assume an exponentially increasing gap width $b(t) = b_o \mathrm{e}^{\hat{a}t}$, where $\hat{a}$ is a control parameter. This physical problem is governed by the set of following equations [8–10, 17, 19]:

$$\boldsymbol{\nabla} \cdot \mathbf{u} = -\frac{\dot{b}(t)}{b(t)} \tag{1}$$

$$\boldsymbol{\nabla}(p + Q) = -\frac{12\mu}{b^2}\mathbf{u} + \rho\hat{\omega}^2\mathbf{x} + 2\rho\hat{\omega}\mathbf{e}_z \times \mathbf{u} + \boldsymbol{\nabla} \cdot (\hat{\delta}(\boldsymbol{\nabla}c)(\boldsymbol{\nabla}c)^{\mathrm{T}}) \tag{2}$$

$$\frac{\partial c}{\partial t} + \mathbf{u} \cdot \boldsymbol{\nabla}c = D\boldsymbol{\nabla}^2 c \tag{3}$$

Equation (1) expresses a modified incompressible condition, which accounts for the lifting or pressing of the upper plate [17]. The gap-averaged velocity is $\mathbf{u}$, while the overdot denotes total time derivative. A generalized Darcy's law is expressed by Equation (2), where p is the hydrodynamic pressure, and Q is the additional pressure due to Korteweg stresses [19–23]. In addition to the conventional viscous term on the right-hand side of this equation, the extra three terms are the centrifugal forces, Coriolis forces and Korteweg stresses, respectively. The concentration of lighter fluid is represented by c, and μ denotes the viscosity, $\hat{\omega}$ the angular speed, $\mathbf{x}$ the position vector on x–y plane, $\mathbf{e}_z$ the unit vector in z-direction, and $\hat{\delta}$ the Korteweg stresses coefficient. The superscript T denotes a transpose. The concentration equation is given by Equation (3), where D is the constant diffusion coefficient.

The density and viscosity variations of the mixture are expressed as

$$\rho(c) = c\rho_{\mathrm{l}} + (1 - c)\rho_{\mathrm{h}} \tag{4}$$

$$\mu(c) = \mu_{\mathrm{l}}\mathrm{e}^{R(1-c)}, \quad R = \ln(\mu_{\mathrm{h}}/\mu_{\mathrm{l}}) \tag{5}$$

where R is the viscosity parameter. In order to render the governing equations dimensionless, we take the diameter D_o of the droplet and the density difference $\Delta\rho = \rho_{\mathrm{h}} - \rho_{\mathrm{l}}$ as the characteristic scales. Since the simulation is carried in the reference frame rotating with the cell, a centrifugal-induced time, $12\mu_{\mathrm{l}}/b_o^2\Delta\rho\hat{\omega}^2$, is taken as a characteristic time scale. By further scaling with viscosity μ_{l} and pressure $\Delta\rho\hat{\omega}D_o^2$, a characteristic velocity scale $b_o^2\Delta\rho\hat{\omega}^2 D_o/12\mu_{\mathrm{l}}$ is obtained. By making the governing equations dimensionless, we obtain the dimensionless

parameters, such as the Peclet number Pe, which can be interpreted as the dimensionless rotating speed, the viscosity parameter R representing the viscosity contrast, the Reynolds number Re, which includes the effect of the Coriolis forces, the dimensionless Korteweg constant δ that stands for the effects of Korteweg stresses, the gap width parameter a, which can express the variety of the dimensionless speed in the gap spacing, and take the forms

$$Pe = \frac{\Delta\rho b_o^2 \hat{\omega}^2 D_o^2}{12\mu_l D}, \quad R = \ln\frac{\mu_h}{\mu_l}, \quad Re = \frac{\Delta\rho b_o^2 \hat{\omega}}{12\mu_l}, \quad \delta = \frac{\hat{\delta}}{\Delta\rho\hat{\omega}^2 D_o^4}, \quad \hat{a} = \frac{12a\mu_l}{\Delta\rho b_o^2\hat{\omega}^2} \tag{6}$$

The velocity is further split into a divergence-free component $\mathbf{u}_f$, which is the velocity of the constant spacing, and an axisymmetric divergent radial velocity $\mathbf{u}_d(r)$ caused by the gap variation [19], so that

$$\mathbf{u} = \mathbf{u}_f + \mathbf{u}_d \tag{7}$$

$$\nabla \cdot \mathbf{u}_f = 0 \tag{8}$$

$$\nabla \cdot \mathbf{u}_d = -a \tag{9}$$

The divergent radial velocity is obtained directly from Equation (9) as $\mathbf{u}_d = -a\mathbf{r}/2$, which is a potential field. The divergence-free component $\mathbf{u}_f = (u_f, v_f)$ can be obtained by solving the equations of streamfunction ψ and vorticity ω, expressed as

$$u_f = \frac{\partial\psi}{\partial y}, \quad v_f = -\frac{\partial\psi}{\partial x} \tag{10}$$

$$\nabla^2\psi = -\omega \tag{11}$$

$$\omega = -R\nabla\psi\cdot\nabla c - \frac{1}{e^{-2at}\mu}\left(y\frac{\partial c}{\partial x} - x\frac{\partial c}{\partial y}\right) - \frac{2Re}{e^{-2at}\mu}\left(u\frac{\partial c}{\partial x} + v\frac{\partial c}{\partial y} + \rho a\right)$$
$$-\frac{\delta}{e^{-2at}\mu}\left(\frac{\partial c}{\partial x}\left(\frac{\partial^3 c}{\partial x^2\partial y} + \frac{\partial^3 c}{\partial y^3}\right) - \frac{\partial c}{\partial y}\left(\frac{\partial^3 c}{\partial y^2\partial x} + \frac{\partial^3 c}{\partial x^3}\right)\right) \tag{12}$$

Since the effects of centrifugal forces and Coriolis forces are more enhanced as the fingers grow further away from the rotating axis, the computational domain is enlarged twice of the previous studies [8, 9] to account for significant Coriolis forces. Boundary conditions are prescribed as follows:

$$x = \pm 2: \ \psi = 0, \quad \frac{\partial c}{\partial x} = 0 \tag{13}$$

$$y = \pm 2: \ \psi = 0, \quad \frac{\partial c}{\partial y} = 0 \tag{14}$$

The initial conditions are assumed as a circular shape bounded by a steep concentration gradient in a form of error function. For obtaining extremely fine structures of fingers, a highly accurate pseudospectral method is employed. To solve the streamfunction equation by

a pseudospectral method, a Galerkin-type discretization using cosine expansion is employed in the streamwise direction

$$\psi(x, y, t) = \sum \hat{\psi}_k(y, t) \cos[2\pi k x] \tag{15}$$

$$\omega(x, y, t) = \sum \hat{\omega}_k(y, t) \cos[2\pi k x] \tag{16}$$

In the normal direction, discretization is accomplished by sixth-order compact finite differences. Vorticity equation is evaluated by sixth-order compact finite difference schemes. The spatial derivatives in the concentration equation are discretized by sixth- and fourth-order compact finite difference schemes for diffusion terms and convection terms, respectively. A fully explicit third-order Runge–Kutta procedure on time is employed to solve concentration equation and advance in time as

$$\frac{\partial c}{\partial t} = F(c) \tag{17}$$

so that

$$c_{i,j}^{k} = c_{i,j}^{k-1} + \Delta t[\gamma_k F(c_{i,j}^{k-1}) + \eta_k F(c_{i,j}^{k-2})] \tag{18}$$

where $\gamma_1 = 8/15, \eta_1 = 0;\ \gamma_2 = 5/12, \eta_2 = -17/60;\ \gamma_3 = 3/4, \eta_3 = -5/12$.

The numerical scheme is largely similar to the one used for earlier investigations on planar fronts [24–26], which had been validated by comparing growth rates of small perturbations with linear stability results. In addition, the numerical code had also been employed recently to further study the fingering formation on a similar rotating Hele–Shaw flow with significant influences of the Korteweg stresses [23]. The numerical results agree excellently with the correspondent immiscible experimental findings both qualitatively and quantitatively. All these relevant validations for similar flow fields can serve as the creditability of the numerical method employed in the present study. More details on the implementation and quantitative validation of these schemes are provided in References [24–26].

3. RESULTS AND DISCUSSIONS

We begin our investigation by a systematic study of the concentration images obtained for different values of the control parameters: Peclet number Pe, viscosity parameter R, Korteweg constant δ and gap width parameter a. Coupling with significant Coriolis effects, the influences of these control parameters will be evaluated first in a constant gap width cell followed by a time-dependent gap cell. In order to account for the significant effect of Coriolis forces, we keep the Reynolds number fixed at $Re = 1.5$, which is the typical value in the practical spin coating procedure, in this study. Furthermore, a constant density ratio at $\rho_h/\rho_l = 2$ is applied for cases with a non-zero gap width parameter to simplify the problem.

3.1. Reference case

A representative calculation of a droplet in constant gap-spacing cell, but assuming absence of Korteweg stress, i.e. $a = 0$ and $\delta = 0$, for $Pe = 7000$, $R = 2$ is described. The R-value indicates

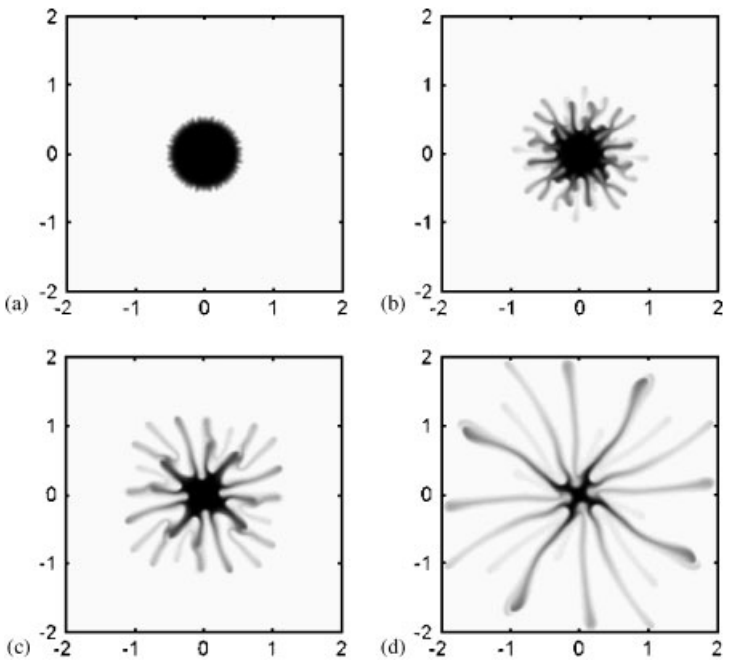

Figure 1. $Pe = 7000$, $R = 2$, $Re = 1.5$, $a = 0$, $\delta = 0$; concentration images at: (a) $t = 5$; (b) $t = 15$; (c) $t = 20$; and (d) $t = 28$. Very vigorous interfacial instability is triggered by the strong centrifugal force, giving rise to a characteristic fingerings pattern: fingers growing, nonlinear tip-splitting, fingers merging and multi-layer fingering. Due to the nature in which the centrifugal force is proportional to radial distance, these fingering instabilities are further enhanced at later time. Besides, the pattern shows the counter-clockwise trend due to the influences of strong Coriolis forces.

that the droplet is about 7.4 times more viscous than the environment. Figure 1 displays the time sequences of the concentration fields. First, there is a latency period when the interface remains circular. After this period, the interface develops small ripples, which indicates the initiation of instability. Very vigorous interfacial instability is triggered by the strong centrifugal force in time, giving rise to a characteristic fingerings pattern: fingers growing, nonlinear tip-splitting, fingers merging and multi-layer fingering. Due to the nature in which the centrifugal force is proportional to radial distance, these fingering instabilities are further enhanced at later time. At $t = 15$, slimmer structures associated with fingers tip-splitting and merging are observed. This merging of fingers is more significant by the effect of the Coriolis force. As the orientation of the Coriolis force applies tangentially to the droplet circumference, this leads to the merging events between the closely adjacent fingers. Because one of them has denser concentration, the adjacent fingers rotating in relative tangential speed tend to merge together. At later time, i.e. $t = 20$, and 28, the concentration images clearly show the counter-clockwise trend and multi-layers of fingers. While the concentration of the far outer fingers disperses significantly, some of them obtain enough flux from the droplet centre and progressively stretch outward, the others gradually disappear. Simultaneously, the inner fingers of a new layer grow fast because of the stronger centrifugal force and Coriolis force

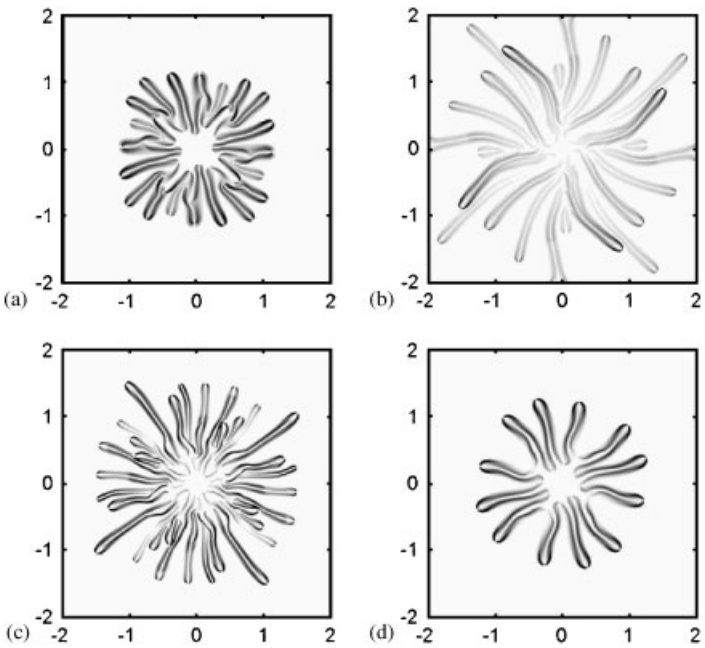

Figure 2. $Re = 1.5$, $a = 0$; vorticity contours at $t = 20$ for: (a) $Pe = 7000$, $R = 2$, $\delta = 0$; (b) $Pe = 7000$, $R = 1$, $\delta = 0$; (c) $Pe = 14\,000$, $R = 2$, $\delta = 0$; and (d) $Pe = 7000$, $R = 2$, $\delta = -10^{-5}$. The vorticity contours clearly show the apparent multi-layer fingers' fronts. However, the pattern including Korteweg stresses effects shows only single-layer fingering and the interfacial instabilities are significantly restrained.

induced by their dense concentration. These new fingers will stretch outward by following the old tracks and even surpass the old ones. Contours of absolute values of vorticity, displayed in Figure 2(a), clearly confirms the multi-layer fingers' fronts and the counter-clockwise trend at later time $t = 20$.

3.2. *Effects of control parameters in a constant gap width cell*

For a heavier and more viscous droplet, the centrifugal force provides an unstable outward driving force, while the viscous effect tends to stabilize the contacting front [8]. The occurrence of instability is decided by the competition of unstable centrifugal force and stable viscous damping. In Figure 3 we keep the same physical parameters used in Figure 1, but decrease the value of the viscosity parameter to $R = 1$. Compared to the reference case, the fingerings are far more vigorous at $t = 15$. In agreement with the previous study [8], a lower viscosity parameter provides less stable damping effects. Thus, it leads to more vigorous fingerings. Note that the pronounced counter-clockwise tilting of the fingers is caused by the effect of the stronger Coriolis force. These concentration images associated with the vorticity contours shown in Figure 2(b) clearly show the apparent multi-layer fingers' fronts at later time. In this lower viscosity contrast case, the fingers grow, stretch outwardly, and diffuse transversely, which leads to the far outer fingers to disperse quickly and form the multi-layer topologies. However, the front of fingers with dense concentration will disappear later on. This interesting multi-layer front is similar to the findings of the immiscible case [4].

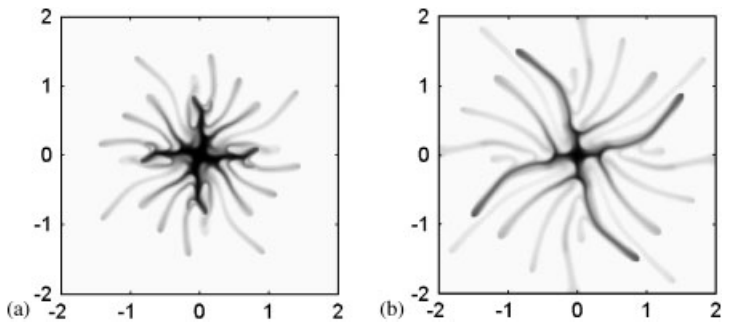

Figure 3. $Pe = 7000$, $R = 1$, $Re = 1.5$, $a = 0$, $\delta = 0$; concentration images at: (a) $t = 15$; and (b) $t = 20$. A lower viscosity parameter provides less stable damping effects, and leads to more vigorous fingerings and the clearly counter-clockwise tilting of the fingers.

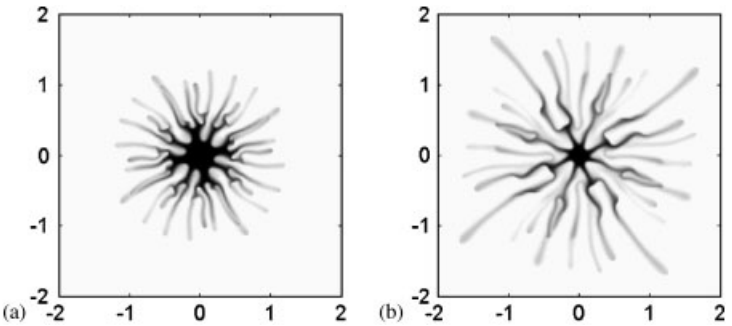

Figure 4. $Pe = 14\,000$, $R = 2$, $Re = 1.5$, $a = 0$, $\delta = 0$; concentration images at: (a) $t = 15$; and (b) $t = 20$. The development of more vigorous branches is observed, since the stronger centrifugal force induces more vigorous interfacial instability.

We now turn to the investigation of the role played by the Peclet number. As shown in the reference case, we keep the viscosity parameter at $R = 2$, but increase the value of the Peclet number to $Pe = 14\,000$, meaning weaker diffusive effects or faster rotating speed. As expected, the stronger centrifugal force induces more vigorous interfacial instability as shown in Figure 4. We observe that the development of more vigorous branches remains to the later stage ($t = 20$). An interface with significant multi-layers is resulted. In addition, the new layer is much more ramified. These phenomena can also be observed by contours of vorticity, depicted in Figure 2(c). The new layer presents outgoing fingers, which develop a peculiar fork-like shape, which is also identified in immiscible situation [7], at $t = 20$. Besides, compared to the reference case, the fingering pattern clearly shows a rotational trend because of the stronger Coriolis effects induced by the faster rotating speed.

The role played by Korteweg stresses is discussed now. From the morphological similarities between the observed miscible patterns including Korteweg stresses, and the structures obtained in related immiscible flows [10, 19, 21, 22], it has been concluded to treat Korteweg

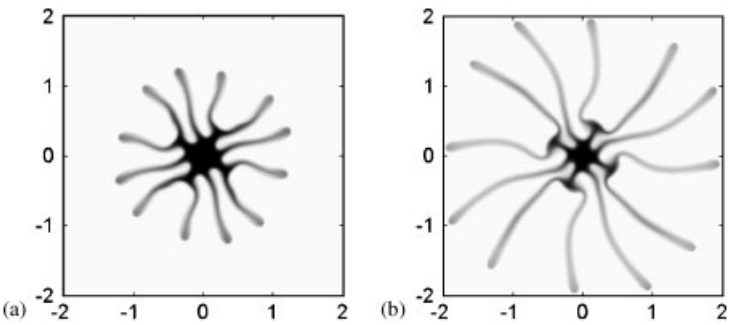

Figure 5. $Pe = 7000$, $R = 2$, $Re = 1.5$, $a = 0$, and $\delta = -10^{-5}$; concentration images at: (a) $t = 20$; and (b) $t = 24$. The pattern shows only single-layer fingering and the interfacial instabilities are clearly restrained. It reveals the stabilizing role playedby the Korteweg stresses.

stresses as an effective surface tension on mixing miscible interfaces. The influences of Korteweg stresses on the pattern evolution are shown in Figure 5, as the same physical parameters in Figure 1 except $\delta = -10^{-5}$. The pattern reveals the stabilizing role played by Korteweg stresses. Furthermore, the pattern shows only single-layer fingering, and the interfacial instabilities are significantly restrained. One of the most remarkable features of the pattern's temporal evolution is the absence of competition between adjacent fingers. Also, the number of growing fingers is not changed during the development of the pattern. These phenomena, also observed by contours of vorticity in Figure 2(d) as well, are in line with the previous studies of a droplet in different flow fields [10, 19, 21, 22].

3.3. Simulations of a time-dependent gap cell

The value of gap width parameter a represents the variety of the gap spacing. A negative parameter a represents a pressed cell while lifted, if a is positive. It is interesting to point out that the situation of a pressing cell is quite similar to the spin coating without injection. Considering the continuously decreasing thickness of coating layer due to outward spray during the spin coating process, a pressing cell gap is analogous to the practical spin coating. First, in the pressed case, we keep the same physical parameters used in Figure 1 but set the value $a = -0.035$. It is known that displacement by a more viscous fluid leads to a stable interface. So, when the upper plate is pressed at a certain rate, the outward flow of a more viscous fluid provides stable force. Concentration images displayed in Figure 6(a) shows that the interfacial fingerings are suppressed significantly and the miscible interface is found to be more stable. The fingers exhibit a single layer and gradually disperse with the droplet, stretch outward and eventually disappear. At last, it results in a much smoother interface that reveals a fully stable pattern. If the gap width parameter is raised to even higher $a = -0.05$, cf. Figure 6(b), a totally stable mixing front is observed. The squeezing droplet remains nearly circular during the whole pressing process. An interesting comparison of the present pressing cell to the situation with injection [9] can be addressed. While additional radial velocities are provided by these two situations and lead to stabilizing effects, the topologies of the final interfaces appear with apparent differences, i.e. a nearly circular droplet in Figure 6(b) at the present pressing cell case versus an apparent body distortion with injection [9]. These

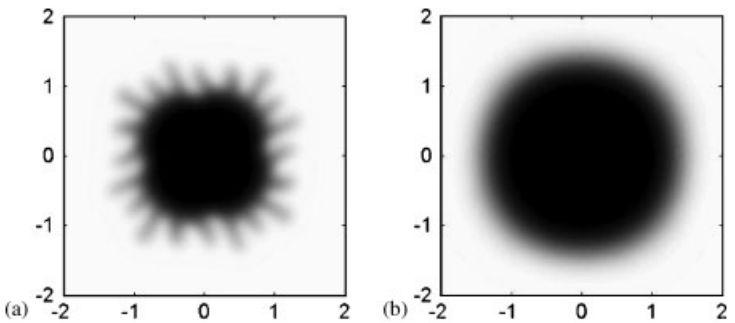

Figure 6. $Pe = 7000$, $R = 2$, $Re = 1.5$ and $\delta = 0$ at $t = 42$; concentration images for: (a) $a = -0.035$; and (b) $a = -0.05$. The higher pressing rate provides more stable effects by additional outward flows.

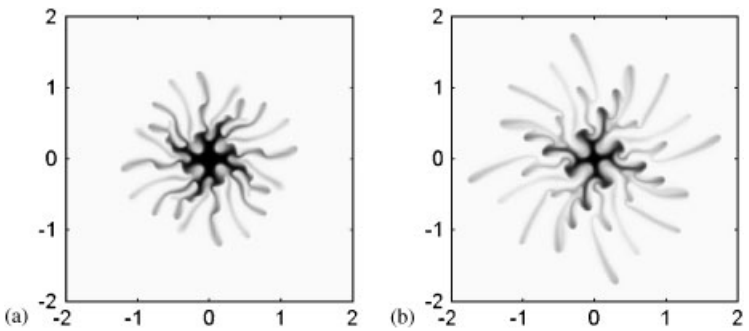

Figure 7. $Pe = 7000$, $R = 2$, $Re = 1.5$, $a = 0.015$, and $\delta = 0$; concentration images at: (a) $t = 15$; and (b) $t = 17$. The beautiful interfacial patterns show the fingers rotating counter-clockwise with drops' emission in the tangential direction.

inconsistent topologies are attributed to the different distributions of the radial velocities. The magnitudes of radial velocity caused by injection are inversely proportional to the distance away from the origin and decay as the fingers further grow. As a result, the interface is predominated by the centrifugal forces and Coriolis forces at later stage. It explains the distortion of the droplet. Nevertheless, at the present pressing cell, the radial velocity is proportional to the radial distance. For a significantly larger pressing rate, the interface is primarily controlled by the radial velocity caused by pressing and remains nearly circular for all times.

Next, we turn to the simulations in a lifting Hele–Shaw cell. The gap width parameter is changed to $a = 0.015$ as shown in Figure 7. This lifting puts the droplet under a lateral straining flow. A less viscous flow displaces the more viscous droplet, which leads to fingering enhancement. It results in the penetration of few inward (wide and round) fingers toward the droplet centre, and extrudes the outgrowing fingers with the nodes of dense concentration. They induce the strong centrifugal force and Coriolis force, which move fingers fast outwardly and tangentially. Great enhancement of interfacial instabilities and the development of more vigorous fingering are observed. The beautiful interfacial patterns show the fingers rotating

counter-clockwise with drops' emission in the tangential direction. These results show exciting dynamical and morphological patterns.

3.4. *Quantitative analysis of tilting angles of fingers*

The above simulations have confirmed the general expectations, such that more vigorous fingerings are triggered by a faster rotating speed, a lower viscosity contrast, stronger surface tension effects and a higher lifting rate. Also shown is the lack of fingering competitions and nonlinear fingering behaviours, such as splitting, merging and multi-layer, for stronger Korteweg stresses. These relatively simple fingering patterns at stronger Korteweg stresses provide better samples to evaluate the quantitative influences of Coriolis forces, such as the tilting angles θ. Figure 8 shows a typical pattern obtained at $Pe = 14\,000$, $R = 1$ and $\delta = -5 \times 10^{-6}$. At $t = 10$, it is clearly observed that all fingers demonstrate the absence of finger competition as well as the nonlinear activities. It is important to note that the morphologies observed in this result are remarkably similar to the ones obtained experimentally and numerically for immiscible flow [4–7]. At $t = 15$, extremely slim fingers turn counter-clockwise due to the effects of the strong centrifugal force and Coriolis force. In order to avoid the emergence of multi-layer fingering for combinations of all the control parameters simulated, in this study, only simulations with significant Korteweg stresses, i.e. $\delta = -10^{-5}$ will be used in the quantitative evaluation of Coriolis effects.

Shown in Figures 9(a) and (b) are the corresponding polar representations of the representative interfaces, taken as the concentration contours $c = 0.95$, for a particular case of $Pe = 7000$, $R = 2$ and $Re = 1.5$ as concentration images presented in Figures 5(a) and (b), respectively. The initial flat interfaces are also plotted by the dash-dot lines. Under the influences of significant Coriolis forces, tilting fingertips are clearly observed as time proceeds. At the later time $t = 24$, shown in Figure 9(b), all the fingers oriented toward nearly the same tilting angles. On the other hand, the fingertips keep growing normally without the effects of Coriolis force, cf. $Re = 0$ in Figure 9(c). We further plot the evolution of mean tilting angles for cases with various control parameters in Figure 10. Similar evolving histories are found for all the three

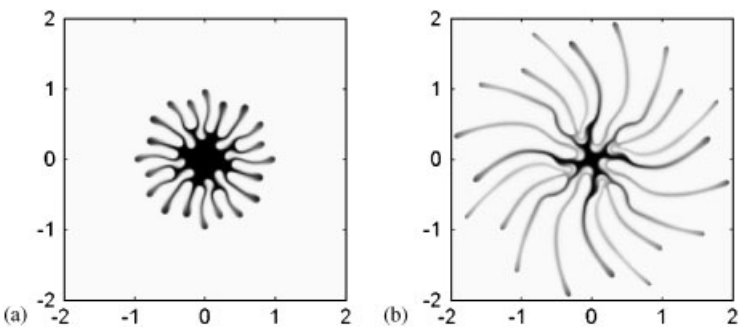

Figure 8. $Pe = 14\,000$, $R = 1$, $Re = 1.5$, $a = 0$, $\delta = -5 \times 10^{-6}$; concentration images at: (a) $t = 10$; and (b) $t = 15$. At $t = 10$, it is clearly observed that all fingers demonstrate the absence of finger competition. At $t = 15$, extremely slim fingers turn counter-clockwise due to the effects of the strong centrifugal force and Coriolis force.

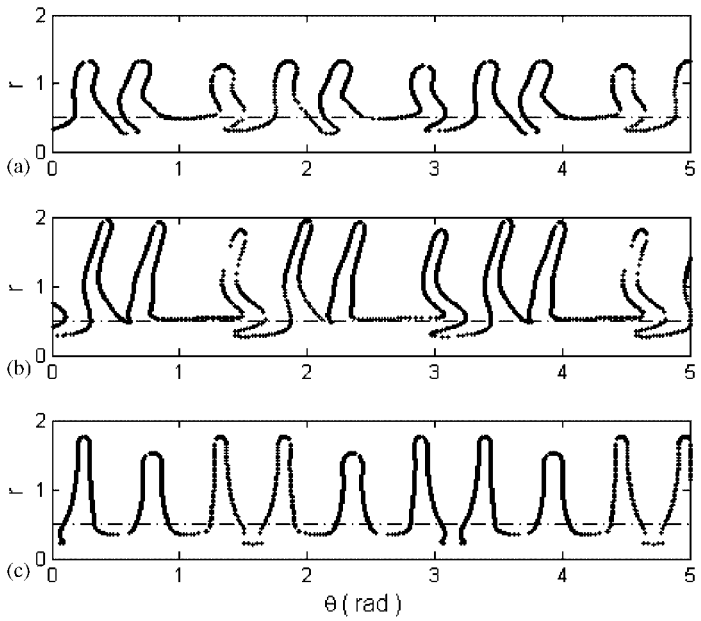

Figure 9. Polar representation of the interfaces: (a) as corresponding concentration image shown in Figure 5(a); (b) as corresponding concentration image shown in Figure 5(b); and (c) for $Re = 0$ at $t = 20.5$. At the later time $t = 24$ shown in (b), all the fingers oriented toward nearly the same tilting angles. On the other hand, the fingertips keep growing normally without the effects of Coriolis force, cf. $Re = 0$ in (c). The initial flat interfaces are also plotted by the dash-dot lines.

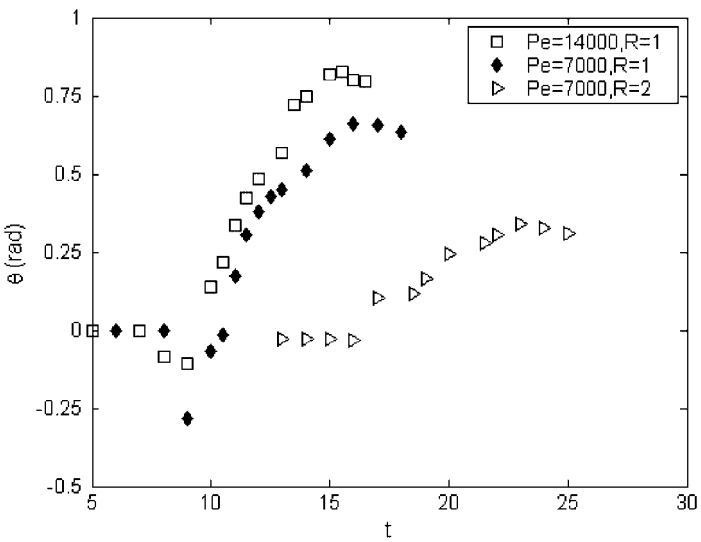

Figure 10. $Re = 1.5$, $a = 0$, and $\delta = -10^{-5}$; time evolution of mean tilting angles of fingers for various control parameters. The tilting angles show significant growths, and reach their maximal when the fingers arrive shortly before to the computational boundaries.

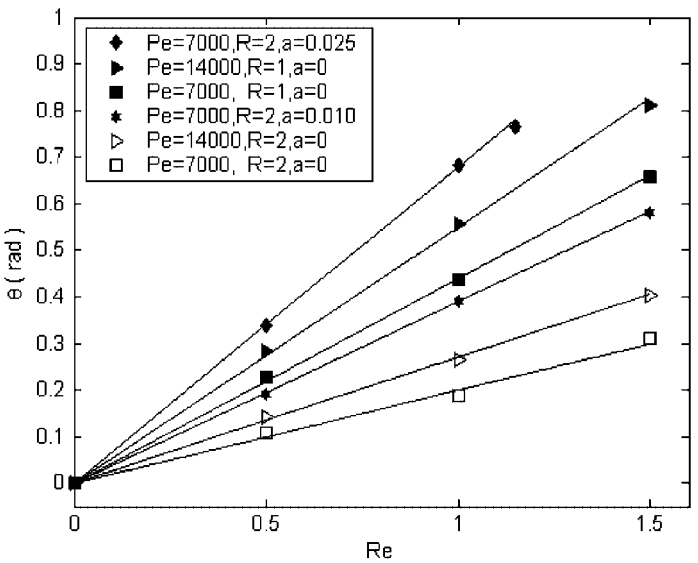

Figure 11. Plot of θ as a function of Reynolds number Re for various parameters. The solid lines are linear fit of the data. The values of θ follow a nearly linear relationship with Re for arbitrary combinations of all the control parameters Pe, R and a.

representative cases. Since the Coriolis forces induce effects by outward fingering growths, the effects of Coriolis force are less significant in the early period, which corresponds the latent period described earlier. Nearly no growths of tilting angles are observed. It should be pointed out that the slightly negative values of tilting angles are mainly caused by the irregular fingering patterns. Due to the nature that the Coriolis force is proportional to radial distance, these effects are further enhanced at the later stage. However, for a miscible flow, the Coriolis force also depends on the local density of fingers as shown in Equation (2), which continuously decreases due to the mixing effects by dispersion and diffusion. As a result, the tilting angles show significant growths until they reach their maxima before the occurrences of strong mixing. Subsequently, since the concentration of the far outer fingers disperses significantly, these values decrease slightly when fingers fully approach the computing boundary. At the time, these fingers have stretched outward and their length have reached nearly the triple of the droplet radius. These tilting angles are then taken to represent the quantitative influences of Coriolis forces. We delineate these values of tilting angles in Figure 11. It is interesting to find out that the values of θ follow a nearly linear relationship with Reynolds numbers for arbitrary combinations of all the control parameters Pe, R and a. Furthermore, these linear lines converge to the origin as Re approaches zero. The nice convergence to the origin indicates the appropriateness of present quantitative evaluation. Finally, we evaluate the slopes as a function of the relevant control parameters and plot them in Figure 12. We estimate the correlation between the relevant control parameters and tilting angles of fingers that can be approximated as

$$\theta = (0.0047\sqrt{Pe}/R + 18.2a)Re \tag{19}$$

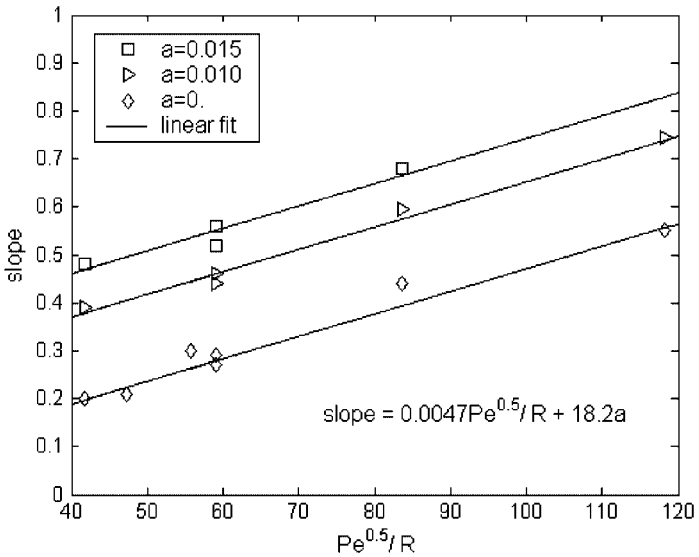

Figure 12. Plot of the slopes as a function of $Pe^{0.5}/R$ for various a. The correlation between the relevant control parameters and tilting angles of fingers can be approximated as $\theta = (0.0047\sqrt{Pe}/R + 18.2a)Re$.

4. CONCLUSION

We have presented highly accurate numerical simulations for miscible displacement in a rotating Hele–Shaw cell. The interfacial instabilities have been analysed systematically. Our analysis explicitly indicates how the relevant control parameters of the system, such as the rotating speed in a dimensionless form of Peclet number Pe, the viscosity contrast parameter R, the miscible interfacial Korteweg stresses constant δ and the gap width parameter a, influence the morphology of the interfacial patterns. We focused on the situations in which Coriolis force, in terms of dimensionless parameter Reynolds number Re, are significant. In line with earlier studies that did not account for sufficient Coriolis forces, we find that more vigorous fingerings are observed at a larger Pe, a lower R, a weaker surface tension constant δ and a faster lifting gap width parameter a. In these cases, more obvious nonlinear behaviours develop, such as tip-splitting, finger merging and multi-layer fingering. On the other hand, the higher pressing rate provides more stable effects by additional outward flows. Furthermore, we investigate the quantitative relationship between the mean tilting angles θ of fingers and the Coriolis effects Re. A nearly linear relationship between the mean tilting angles θ of fingers and the Coriolis effects Re is found for arbitrary combinations of all the relevant control parameters. These linear lines converge nicely to the origin when Reynolds numbers vanish supports the appropriateness of such quantitative evaluations. We estimate the correlation between the control parameters and tilting angles of fingers that can be approximated as $\theta = (0.0047\sqrt{Pe}/R + 18.2a)Re$ for significant Korteweg stresses.

REFERENCES

1. Hill S. Channeling in packed columns. *Chemical Engineering Science* 1952; **1**:247–253.
2. Saffman P, Taylor G. The penetration of a fluid into a porous medium of Hele–Shaw cell containing a more viscous liquid. *Proceedings of the Royal Society of London*, *Series A* 1958; **245**:312–329.
3. Maxworthy T. Experimental study of interface instability in a Hele–Shaw cell. *Physical Review A* 1989; **39**(11):5863–5866.
4. Schwartz L. Instabilities and fingering in a rotating Hele–Shaw cell or porous medium. *Physics of Fluids A* 1989; **1**:167–169.
5. Waters S, Cummings L. Coriolis effects in a rotating Hele–Shaw cell. *Physics of Fluids* 2005; **17**:048101.
6. Carrillo L, Soriano J, Ortin J. Interfacial instability of a fluid annulus in a rotating Hele–Shaw cell. *Physics of Fluids* 2000; **12**(7):1685–1698.
7. Alvarez-Lacalle E, Ortin J, Casademunt J. Low viscosity contrast fingering in a rotating Hele–Shaw cell. *Physics of Fluids* 2004; **16**(4):908–924.
8. Chen C-Y, Wang S. Interfacial instabilities of miscible fluids in a rotating Hele–Shaw cell. *Fluid Dynamics Research* 2002; **30**(5):315–330.
9. Chen C-Y, Liu Y-C. Numerical simulations of miscible fluids on a rotating Hele–Shaw cell with effects of Coriolis forces. *International Journal for Numerical Methods in Fluids* 2005; **48**(8):853–867.
10. Chen C-Y, Wu H-J. Numerical simulations of interfacial instabilities on a rotating miscible magnetic droplet with effects of Korteweg stresses. *Physics of Fluids* 2005; **17**(4):042101.
11. Miranda J. Rotating Hele–Shaw cells with ferrofluids. *Physical Review E* 2000; **62**:2985.
12. Jackson D, Miranda J. Controlling fingering instabilities in rotating ferrofluids. *Physical Review E* 2003; **67**:017301.
13. Gadelha H, Miranda J. Finger competition dynamics in rotating Hele–Shaw cells. *Physical Review E* 2004; **70**:066308.
14. Chen C-Y, Wu H-J. Fingering instabilities of a miscible magnetic droplet on a rotating Hele–Shaw cell. *Journal of Magnetism and Magnetic Materials* 2005; **289**:339–341.
15. Wang W, Chou F. Fingering instability and maximum radius at high rotational Bond number. *Journal of the Electrochemical Society* 2001; **148**(5):G283–G290.
16. Schwartz L, Roy R. Theoretical and numerical results for spin coating of viscous liquids. *Physics of Fluids* 2004; **16**(3):569–584.
17. Shelley M, Tian F-R, Wlodarski K. Hele–Shaw flow and pattern formation in a time-dependent gap. *Nonlinearity* 1997; **10**:1471–1495.
18. Derks D, Lindner A, Creton C, Bonn D. Cohesive failure of thin layers of soft model adhesives under tension. *Journal of Applied Physics* 2003; **93**(3):1557–1566.
19. Chen C-Y, Chen C-H, Miranda J. Numerical study of miscible fingering in a time-dependent gap Hele–Shaw cell. *Physical Review E* 2005; **71**:056304.
20. Hu H, Joseph D. Miscible displacements in a Hele–Shaw cell. *Zeitschrift fur Angewandte Mathematik und Physik* 1992; **43**:626–645.
21. Chen C-Y, Wang L, Meiburg E. Miscible droplets in a porous medium and the effect of Korteweg stresses. *Physics of Fluids* 2001; **13**(9):2447–2456.
22. Chen C-Y. Numerical simulations of fingering instabilities in miscible magnetic fluids in a Hele–Shaw cell and the effects of Korteweg stresses. *Physics of Fluids* 2003; **15**(4):1086–1089.
23. Chen C-Y, Chen C-H, Miranda J. Numerical study of pattern formation in miscible rotating Hele–Shaw flows. *Physical Review E* 2005, submitted.
24. Chen C-Y, Meiburg E. Miscible porous media displacements in the quarter five-spot configuration. Part 1: the homogeneous case. *Journal of Fluid Mechanics* 1998; **371**:233–268.
25. Ruith M, Meiburg E. Miscible rectilinear displacements with gravity override. Part 1: homogeneous porous medium. *Journal of Fluid Mechanics* 2000; **420**:225–257.
26. Meiburg E, Chen C-Y. High-accuracy implicit finite difference simulations of homogeneous and heterogeneous miscible porous media flows. *SPE Journal* 2000; **5**(2):129–137.

